Effects of size constraint on water filling process in nanotube

Lingyi Meng, Qikai Li, and Zhigang Shuai

Citation: The Journal of Chemical Physics **128**, 134703 (2008); doi: 10.1063/1.2883655
View online: https://doi.org/10.1063/1.2883655
View Table of Contents: http://aip.scitation.org/toc/jcp/128/13
Published by the American Institute of Physics

Articles you may be interested in

Effect of quantum partial charges on the structure and dynamics of water in single-walled carbon nanotubes
The Journal of Chemical Physics **125**, 114701 (2006); 10.1063/1.2338305

How fast does water flow in carbon nanotubes?
The Journal of Chemical Physics **138**, 094701 (2013); 10.1063/1.4793396

Water in carbon nanotubes: Adsorption isotherms and thermodynamic properties from molecular simulation
The Journal of Chemical Physics **122**, 234712 (2005); 10.1063/1.1924697

PHYSICS TODAY
WHITEPAPERS

ADVANCED LIGHT CURE ADHESIVES

Take a closer look at what these environmentally friendly adhesive systems can do

READ NOW

PRESENTED BY
MASTERBOND
ADHESIVES | SEALANTS | COATINGS

Effects of size constraint on water filling process in nanotube

Lingyi Meng, Qikai Li,[a] and Zhigang Shuai[b]
Beijing National Laboratory for Molecular Sciences (BNLMS), Key Laboratory of Organic Solids, Institute of Chemistry of the Chinese Academy of Sciences, 100080 Beijing, People's Republic of China

(Received 1 October 2007; accepted 29 January 2008; published online 2 April 2008)

Molecular dynamics (MD) simulation and the potential of mean force (PMF) analysis are used to investigate the structural properties of water molecules near the end of nanotube for the whole process from the initial water filling up to the configuration stabilization inside the carbon nanotubes (CNTs). Numerical simulations showed that when a small-sized nanotube is immersed into the water bath, the size constraint will induce a prevailing orientation for the water molecule to diffuse into the tube and this effect can persist approximately 3.3 Å from the end of CNT. As the structure within the CNTs stabilizes, the ambient structural properties can indirectly reflect their corresponding properties inside the nanotube. Our results also showed that there exists a close correlation between the PMF analysis and the results of MD simulations, and the properties at nanometer scale are closely related to the size-constraint effect. © *2008 American Institute of Physics*.
[DOI: 10.1063/1.2883655]

I. INTRODUCTION

The discovery of carbon nanotubes (CNTs) by Iijima[1] has led to widespread studies of this novel material, and many of its properties have been revealed. Up to now, CNTs can be fabricated in various sizes and shapes, with diameters ranging from less than 1 nm to more than 100 nm. The CNTs can be used as a mould or template for material fabrication,[2–5] serving as channels for transport of fluid (nanofluidics),[6–8] etc. Among the applications, the low reactivity of CNTs with a number of substances and their structural stability have prompted a number of investigations on their suitability as artificial nanopores and ion channels which are essential for living organisms ranging from bacteria to animals and plants.[9]

Many recent experimental and theoretical studies have focused specifically on the structural and thermodynamic properties in the vicinity or interior of CNTs.[6,10–14] For example, despite the hydrophobic nature of CNTs, Hummer *et al.*[6] have reported that water molecules can spontaneously and continuously fill into a nonpolar carbon nanotube with a rather strong hydrophobic character and a one-dimensionally ordered chain of water molecules will be shaped inside the CNT. Studies of water transport through the simple idealized pores of CNTs (Ref. 6) may help understand aspects of molecular scale hydrodynamics and serve as models for transport in biological transmembrane channels. To understand the underlying mechanisms, various kinds of models and theories were devised to describe those diffusion processes and condensation configuration of water inside pristine CNT, such as the continuous-time, single-file random-walk model,[15] traditional molecular dynamics,[16] and the coarse molecular dynamics.[17] When CNT was modified through charged atoms, new distribution patterns and controllable transport of water can be realized.[18–20] Other peculiar ice structures[11] and phase transitions[21] never seen in bulk phase can be also found within the narrow confines of carbon nanotubes, and the structure of the confined water strongly depends on the diameter of the nantubes.[22,23] The water molecules adopt a single-file arrangement in the narrow nanotubes, and as the diameter increases, they become more disordered in a fashion similar to that of the bulk water.[24]

The investigation of these systems consisting of nanosized materials and other medium not only helps us understand the structural and dynamic properties of those medium confined on the nanometer scale but also reveals some special characters of the nanosized materials, in particular, the hydrophobic/hydrophilic behavior.[25–28] Hydrophilic/hydrophobic effects on the nanometer scale play a key role in many important physical or chemical phenomena, such as self-assembly and controllable growth of nanosized materials, stabilization of protein structure, and function in solvent (the famous hydrophobic interaction principle). Computational studies have been conducted for structural properties of water molecules surrounding a CNT.[29] The simulations affirmed that the water at the carbon-water interface is found to have a HOH plane nearly tangential to the interface, and the water radial density profile exhibits the characteristic layering also found in the graphite-water system. The structure of water droplets[30] or clusters[31] confined on the nanometer scale and the capillary effects[32] also have been explored.

To understand the underlying structure feature and the structural evolution at nanometer scale, we resort to the potential of mean force (PMF) analysis. The PMF is a Landau free-energy profile along an order parameter, and it can be determined from the equilibrium statistical distribution function of the system by systematically integrating out all degrees of freedom except the order parameter.[33] The PMF is a useful tool to understand various kinds of structural and dynamic information on reversible processes. However, there exists some difficulties for the calculation of PMF. The first

[a]Electronic mail: qkli@iccas.ac.cn.
[b]Electronic mail: zgshuai@iccas.ac.cn.

 © 2008 American Institute of Physics

obstacle is on how to pick up a reasonable parameter as order parameter for the question concerned when the structure of system is complex, while the second one is that the standard simulation methods do not adequately sample the region in which the system reaches with low probability, leading to inaccurate values for the PMF. To avoid the sampling problem, various methods have been proposed for calculating PMF, for instance, the umbrella sampling and the steered dynamics.[34] Water molecules can spontaneously and continuously fill into a nonpolar carbon nanotube and a quasi-one-dimensional (Q1D) structure of water molecules will shape inside the CNT.[6,11,22–24,35] When only the stable structural properties are concerned, the simple method for PMF calculation can be employed in these cases. In this paper, the PMF is calculated through integrating the mean force as defined in Refs. 36 and 37.

Much efforts have been paid to investigating the configurations and dynamic properties of water molecules surrounding or inside CNTs (as mentioned above), but not in vestibules at the openings of the CNTs. However, during the processes of water filling into the CNTs, the environment in the vestibules where water molecules rearrange their configurations and prepare to diffuse into the pores should deserve our attention. After the stabilization of water structure inside CNTs, study of these transitional regions can also help us understand the properties of water clusters inside pores on the nanoscale. In this work, we present our molecular dynamics (MD) simulations and PMF analysis on studying the structural properties of water molecules in these important ranges.

II. SIMULATION MODEL AND COMPUTATIONAL DETAILS

Our simulations were performed with the GROMACS molecular dynamics package.[38,39] The water is described by the flexible SPC/E model featuring harmonic stretch and bend terms between the oxygen and hydrogen atoms at which the partial charges are located, and the electrostatic interactions are evaluated by the particle mesh Ewald method.[40,41]

We describe the carbon nanotubes using a Morse bond, a harmonic cosine of the bending angle, a twofold torsion potential, and a Lennard–Jones (LJ) 12-6 term as

$$U_{\mathrm{SWCNT}}(r_{ij},\theta_{ijk},\phi_{ijkl}) = K_{Cr}[e^{-\gamma(r_{ij}-r_C)}-1]^2 + \tfrac{1}{2}K_{C\theta}(\cos\theta_{ijk}-\cos\theta_C)^2 + \tfrac{1}{2}K_{C\phi}(1-\cos 2\phi_{ijkl}) + 4\varepsilon_{CC}\left[\left(\frac{\sigma_{CC}}{r_{ij}}\right)^{12}-\left(\frac{\sigma_{CC}}{r_{ij}}\right)^{6}\right], \quad (1)$$

where K_{Cr}, $K_{C\theta}$, and $K_{C\varphi}$ are the force constants for the stretch, bend, and torsion potentials, respectively, and r_C, θ_C, and φ_C the corresponding reference geometry parameters for graphene. The θ_{ijk} and φ_{ijkl} represent all the possible bending and torsion angles and r_{ij} the distances between bonded atoms. ε_{CC} and σ_{CC} are the parameters for LJ term excluding 1-2 and 1-3 pairs. The CNT-water interaction is described by a carbon-oxygen LJ potential[6]

TABLE I. Parameters for interaction potentials needed in the simulations. The parameters are taken from Ref. 29 unless otherwise indicated.

K_{Cr}=478.9 kJ mol^{-1}	r_C=1.418 Å
$K_{C\theta}$=562.2 kJ mol^{-1}	θ_C=120.00°
$K_{C\psi}$=25.12 kJ mol^{-1}	γ=2.1867 Å^{-1}
K_{W_r}[a] =3450 kJ mol^{-1} Å^{-2}	r_W=1.0 Å
$K_{W\theta}$=383 kJ mol^{-1} rad^2	θ_W=109.47°
q_O=−0.8476e	q_H=0.4238e
ε_{CC}[a] =0.4058 kJ mol^{-1}	σ_{CC}[a] =3.361 Å
ε_{OO}[a] =0.6503 kJ mol^{-1}	σ_{OO}[a] =3.166 Å
ε_{CO}[a] =0.5137 kJ mol^{-1}	σ_{CO}[a] =3.262 Å

[a]Provided by the GROMACS package.

$$U_{\text{carbon-water}}(r_{ij}) = 4\varepsilon_{CO}\left[\left(\frac{\sigma_{CO}}{r_{ij}}\right)^{12}-\left(\frac{\sigma_{CO}}{r_{ij}}\right)^{6}\right]. \quad (2)$$

As to the quadrupolar interaction between the carbon atoms and the partial charges on the water hydrogen and oxygen atoms, Walther *et al.*[29] have demonstrated that the quadrupolar moment has a negligible influence on the structural properties of the water, thus it is not included in our simulation. All of the parameters involved in the simulations are summarized in Table I.

The single-walled carbon nanotube (SWCNT)-water system is modeled using the canonical (*NVT*) ensemble, and the periodic boundary conditions are applied in all three spatial directions. However, enough space (around 3.8 nm) is left between the top of SWCNT and the bottom clamped water layer along z direction to avoid unreasonable interaction. The temperature is maintained at 300 K using the Berendsen method. A time step of 1.0 fs is used. The cutoff distances for Coulomb potential and LJ potential are 0.9 nm and 1.0 nm, respectively. The SWCNTs were constructed through rolling up single graphite sheets.[42] The sizes of SWCNTs used in our simulations are listed in Table II.

The simulation process was designed as follows: an uncapped SWCNT of about 4 nm in length and with various diameters, ranging from 8.14 to 20.26 Å, is dipped into water surface as a function of cosine-type (stage 1), then the system holds and relaxes at the maximal dipping position (stage 2). To realize this process, we first froze a layer of water molecules at the bottom of the bath (about 1 nm in thickness) and the top part of the SWCNT (about 1 nm in length) as shown in Fig. 1. It takes about 100 ps for the SWCNT to be fully immersed into a depth of about 2.0 nm

TABLE II. Size of SWCNTs used in the simulations. (m,n) stands for the tube chirality index, D the diameter of the tube in angstroms, and N_C the number of carbon atoms.

Case	(m,n)	D (Å)	N_C
1	(6,6)	8.14	408
2	(7,7)	9.50	476
3	(8,8)	10.86	5.44
4	(9,9)	12.22	612
5	(10,10)	13.60	680
6	(12,12)	16.30	816
7	(14,14)	19.02	952
8	(15,15)	20.26	1020

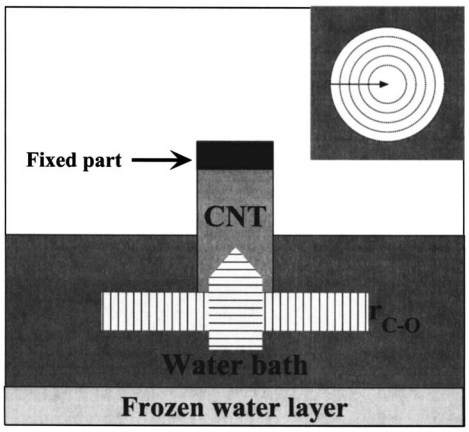

FIG. 1. A schematic of the MD simulation system and integrating regions for PMF calculation. The horizontal hatched area corresponds to the vertical integrating region, while the vertical hatched area corresponds to the radial integrating region (details in inset).

under water surface from its original position. The coordinates and other information were recorded every 0.2 ps. The water box with a number of 12 258 molecules is prepared separately, and the system is equilibrated to obtain the desired temperature (T) of 300 K. The dimension of the water box is approximately $8 \times 8 \times 6$ nm^3.

When a water molecule diffuses along radial direction from the bulk toward the central axle in the mouth region of SWCNT, as shown in Fig. 1, the work done is computed by integrating the mean radial force acting on the water molecule contributed by all other atoms in the system.[37]

$$W(q) - W(q_0) = \int_{q_0}^{q} \langle F(q') \rangle dq', \tag{3}$$

where q_0 is the reference position where the PMF is zero.[37] The mean force distributions along longitudinal axle direction and radial direction were calculated by sampling the force experienced by the water molecules in a binwise scheme, as shown in Fig. 1.

III. RESULTS AND DISCUSSION

As the SWCNT indents to its lowest position and holds, the capillary effects induce a water column to enter into the SWCNT and then growth process follows. When the growth process finishes, the water columns will fully adjust their structures to reach their stable states. The structural properties of water near the end of SWCNT during the growth stage will show different characteristics from those in the stage with stable structures. It can be seen from Fig. 2(a) that the water columns inside most SWCNTs have finished their growth stage at around 500 ps. Therefore, we will later on refer the stage before 500 ps as the growth process for each SWCNT. The simulations corresponding to the growth process were repeated 15 times for each system involved SWCNT with various diameters and the results were averaged. The error distributions for the growing column lengths inside SWCNTs are shown in Fig. 2(b). As shown in the figure, the first dashed line near 200 ps corresponds to the moment when the averaged water column height approximately reaches the outside surface water level, except the (7, 7) SWCNT, the region labeled between the two dashed lines shows relatively large fluctuations, beyond around 350 ps, the fluctuations begin to diminish. At around 500 ps, the fluctuations of water column length inside the SWCNT with diameter larger than that of the (8, 8) nanotube are smaller than 2.0 Å. After 500 ps, the simulations would continue to run for about 10 ns.

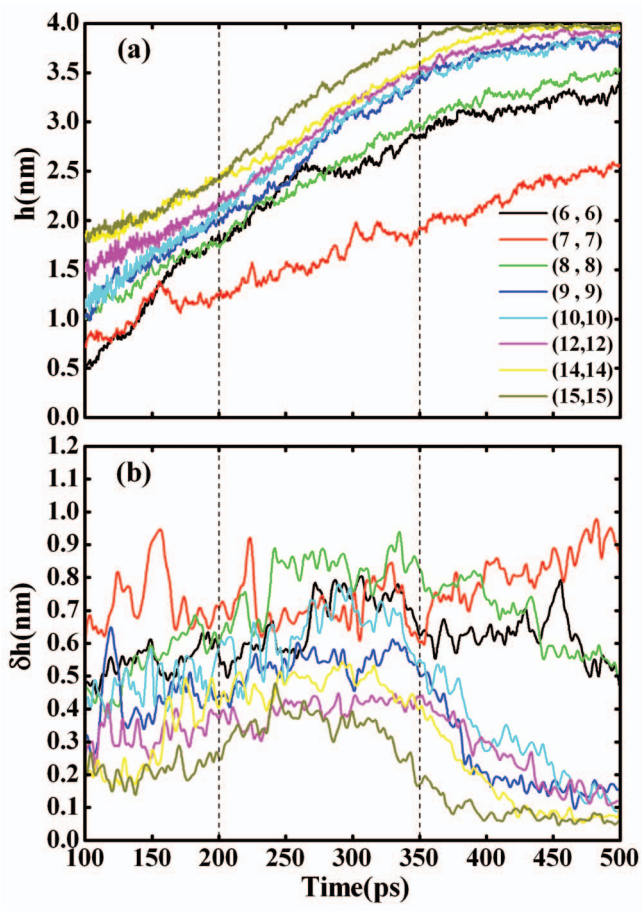

FIG. 2. (Color) Water column lengths within SWCNT (a) and the column length error estimations (b) for systems with different diameters vs time.

To facilitate the discussions over structural properties for the system, we further divide the process into a growth stage and a postgrowth stage. Figure 3 shows the average dipole moment angular distribution for water molecules near the vicinity of the lower end of SWCNT along z direction during the growth process. It is obvious that for the SWCNT with diameter less than around 19.02 Å (corresponding to the (14, 14) SWCNT), there exists a transitional range extending into the water bath by about 0.3 nm. When the water molecules diffuse into this region, a gradually increasing tendency to align with the SWCNT axle will be imposed on these molecules by the size-constraint effects as the water molecules approach the mouth of SWCNT. Moreover, this tendency is retained across the mouth of the SWCNTs during the whole growth process. As the diameter increases, the orientation of water molecule induced by the size-constraint effects gradually disappears. When the diameter reaches

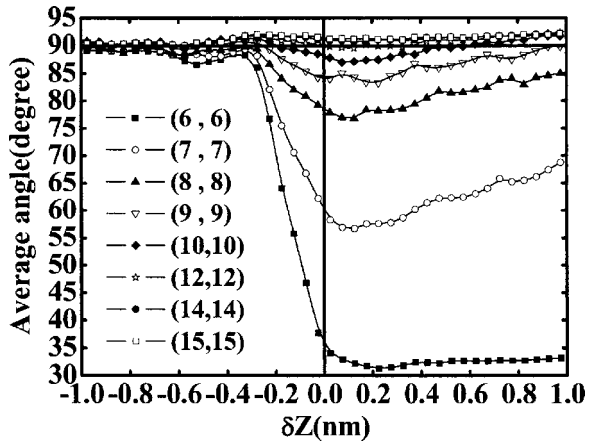

FIG. 3. Average-dipole moment angular distributions for water molecules in region near the lower end of SWCNT along the z direction. The orientation is characterized by the angle between the SWCNT axle and the water dipole moment, and the distance is measured from the lower end of the SWCNT. The negative value stands for statistics in the water bath in front of the lower end of the SWCNT, while the positive value for statistics within SWCNT.

around 19.02 Å [corresponding to the (14, 14) SWCNT], the water dipole alignment tendency is completely lost, as shown in Fig. 3.

Figure 4 shows the density profiles of water molecules in the vestibules of 1 nm length extending from the lower end of SWCNT into the water bath, which is similar to those found by Walther *et al.*[29] The difference lies in that we calculate the distribution along z direction rather than the radial density profile. In the restricted environment in front of the carbon nanotube, the water density profile displays a characteristic layering feature, and the maxima of density profiles at the extending distance of about 3.3 Å is close to the value of σ_{CO} (3.262 Å), which is quite similar to the water radial density profile calculated by Walther *et al.*[29] This characteristic layering gradually weakens as the diameter increases.

For system involved the SWCNT with small diameter, the dipole moment of water molecules in close proximity to the lower end of SWCNT (at $\delta Z \leqslant 2.0$ Å) displays a tendency of alignment to the SWCNT axle. In the same way,

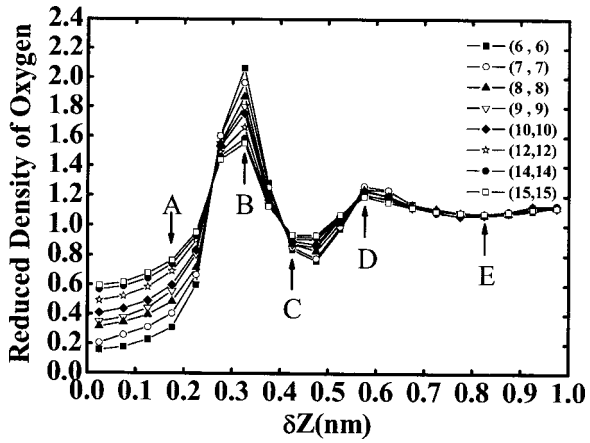

FIG. 4. Water density profile along the z direction for systems with different SWCNT diameters. The water density profile is calculated for vestibules extending from the SWCNT's lower end into the bulk water by 1.0 nm, where ρ_0 is the density of the bulk water. The arrows indicate the centers of the bins used in the following water dipole moment distributions.

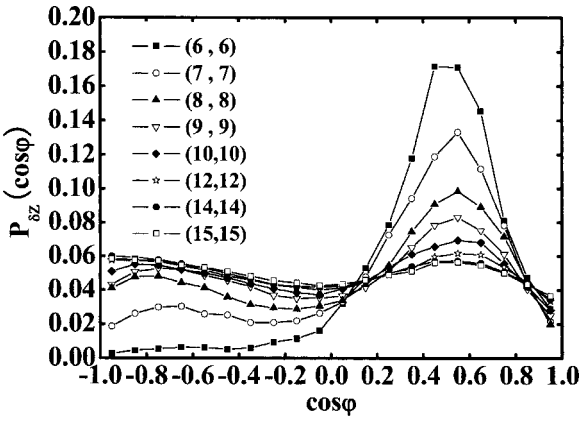

FIG. 5. The water dipole moment distribution for a water slab in systems with different SWCNT diameters. The slab has a thickness of 0.5 Å and a radius equals that of the SWCNT. The distance from the slab to the lower end of the SWCNT is 2.0 Å with its location indicated by label A in Fig. 4.

this alignment tendency weakens as the diameter increases, as shown in Fig. 5. The other relatively weak peak corresponds to the appearance of dipole moment angles $>90°$, as shown in Fig. 5, and this peak tends to shift to the bigger angle direction as the diameter increases.

The orientation distributions of water molecules for different SWCNT diameters and extending regions are shown in Fig. 6. At the maximum of density profile, the water molecules have a tendency to form a profile which is approximately tangential to the lower end of SWCNT. However, small deviations exist for different SWCNTs. The profile maxima describing the orientation distributions of water molecules tend to shift from the angles $<90°$ to the angles $>90°$ as the diameter increases, as shown in Fig. 6(a). These deviations remind us that the size-constraint effects are still in play in this location. At an extending distance of around 4.25 Å which corresponds to the point where local density reaches minimum, the distribution of water dipole moment along the SWCNT axle reaches maximum for angles $>90°$. The water molecules at the second peak in the density profile show an unfavorable tendency to form a dipole moment profile tangential to the lower end of SWCNT. The behavior for the second peak is different to the one for the first peak, and the distribution discrepancy of dipole moments for the water molecules diminishes as the extending distance increases, in the mean time the bulk properties gradually prevail. If the extending distance is larger than around 3.3 Å, the variations of water dipole moment distributions along the SWCNT axle show very similar behavior for SWCNTs with different diameters, as shown in Fig. 6.

As discussed above, the region strongly impacted by the size-constraint effects is limited to the close vicinity near the lower end of narrow SWCNT (at $\delta Z \leqslant 2.0$ Å), and it seems that an orientation adjustment occurs in this region since the relative position of hydrogen atom has negligible effect on the CNT-water interaction energy. The water molecules entering the region near the lower end of SWCNT tend to adopt a special orientation before further entering into the pore region of nanotube. Since the region near the lower end of SWCNT is a source of water column growth inside the chan-

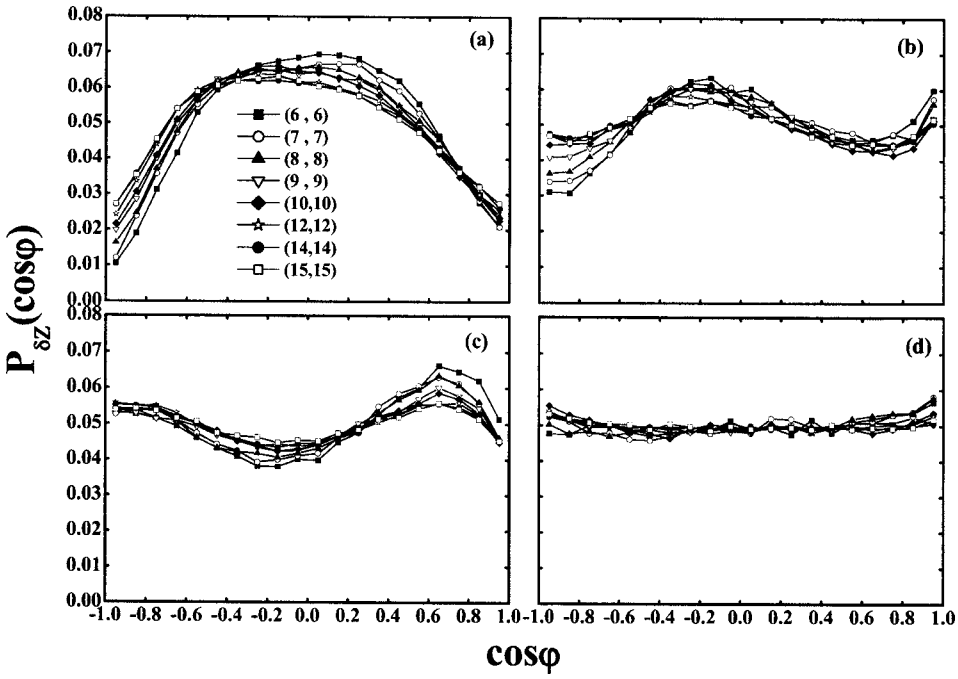

FIG. 6. Orientation distributions of the water dipole moments for systems with different SWCNT diameters at different extending distances. The distribution (a) corresponds to the location labeled by B in Fig. 4, the distribution (b) to location C, the distribution (c) to location D, and the distribution (d) to location E in Fig. 4. The location B corresponds to the first peak, the C to the first minimum, the D to the second peak, and the E to the bulk phase.

nel, the orientation of water molecules in this region determines the arrangement of the molecules that first enter into the SWCNT.

When the water molecules inside SWCNT were fully relaxed and rearranged, the corresponding properties can be determined by the structure formed inside the SWCNT, and they can be quite different from those in the water column growth stage. For example, in the close proximity to the lower end of narrow SWCNT, the tendency of alignment to the SWCNT axle for the dipole moment of water molecules will disappear, and the originally weak peak in the two-peak profile observed in Fig. 5 will be enhanced in the postgrowth stage. In this postgrowth stage, for the very narrow carbon nanotubes, the water molecules can form Q1D structures that might constitute a new phases of ice, different from the 15 polymorphic phases of bulk ice identified experimentally thus far.[43,44] For the SWCNT with a diameter of around 8 Å, a one-dimensionally ordered chain of water molecules will replace the water column inside the SWCNT, as shown in Fig. 7. The Collective flip (the angle of water dipole moment with the z axle changes from angle $<90°$ to angle $>90°$ or vice versa) may occur for this type of chain structure inside the SWCNT as the evolution time is long enough. As the diameter of SWCNT grows, the Q1D chain structures evolve with more complexity and can maintain for a long time. When the diameter of SWCNT reaches around 9.5 Å, the water molecule pairs begin to form, as shown in Fig. 7. In this two-column structure, one chain is associated with upward dipole orientation and the other with a downward orientation. In the case of (8, 8) and (9, 9) SWCNTs, the Q1D n-gonal structures similar to those observed in Refs. 11, 22, and 24 begin to form. However, the perfectness of the hexagonal lattice formed inside (9, 9) SWCNT is higher than that of the tetragonal lattice inside (8, 8) SWCNT, this phenomenon is in good conformance with the result reported by Mashl *et al.*[24] As the diameter of the SWCNT further increases, the water molecules can easily diffuse into the interior of the tubelike structure formed by water molecules, and these configurations will gradually approach the liquidlike phase. These convince us that the phase diagram for the water confined in the nanosized structure is different from the one for the bulk.[45–47] When the diameter is larger than around 10.86 Å [for (8, 8) SWCNT], the average angle between the dipole moment and SWCNT's axle for water molecules inside the SWCNT is over 90°, which is different from those for water molecules near the lower end of SWCNT in the growth stage.

To understand the structural evolution observed in the simulations, we resort to the PMF calculations along the tube

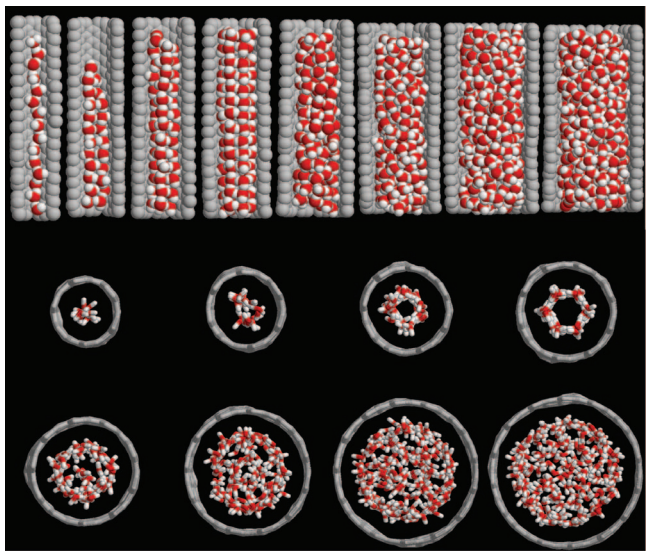

FIG. 7. (Color) Top and lateral views of representative simulation snapshots for water molecules inside SWCNTs. From left to right figures are for water inside (6, 6), (7, 7), (8, 8), (9, 9), (10, 10), (12, 12), (14, 14), and (15, 15) SWCNTs. The red spheres represent oxygen atoms and white spheres represent hydrogen atoms.

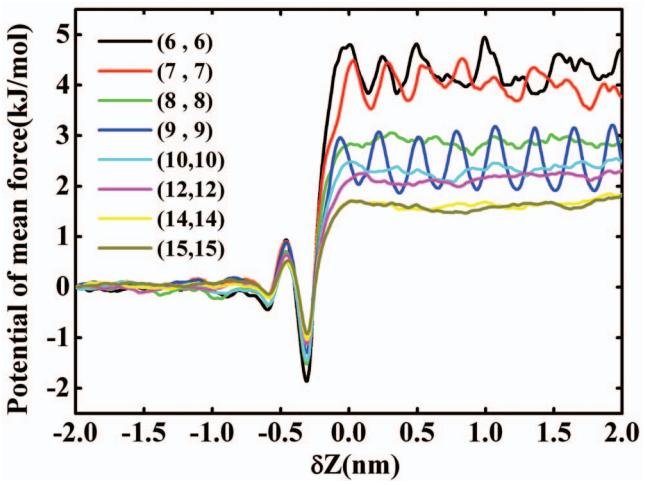

FIG. 8. (Color) The PMF of water along the axle direction of SWCNT with different diameters.

axle and the radial direction in the close vicinity near the lower end of SWCNTs. Figure 8 shows the PMF curves along the tube axle with various SWCNT diameters. The profiles show that except the (9, 9) SWCNT, the smaller the diameter of SWCNT is, the higher the energy barrier for encapsulating a water molecule into the interior of SWCNT, and the larger the energy fluctuation experienced by the water molecules inside the SWCNT. When the diameter reaches around 19.02 Å [corresponding to the (14, 14) SWCNT configuration], the energy barrier and energy fluctuation are small enough for the water molecules to easily diffuse into the pore region of SWCNT. The PMF curve along the tube axle for the (9, 9) SWCNT is an exception for its highly cyclicity inside the tube. This could be the reason for the highly ordered structure formed inside the (9, 9) SWCNT. As is known, the PMF calculated here is a measure of the reversible work for pulling a water molecule from a location to another one in the postgrowth stage. The configurations in the growth stage, which obviously deviate from those stable ones in the postgrowth stage, cannot be effectively sampled in the calculations. Therefore, the PMF results calculated in our simulations cannot be directly used to analyze those dynamical properties in the growth stage or water filling process; however, the calculations can provide an estimation over the relative energy barriers for the water molecules entering into the channels when comparing different SWCNT sizes. As a result, the structural information of water clusters in the postgrowth stage can be reflected though the PMF calculations.

Other structural features can be explained by employing the PMF analysis along the radial direction. For example, for the (9, 9) SWCNT, the distance between the two neighboring minima of the PMF curve along the radial direction in the mouth region of SWCNT is around 0.3 nm, as shown in Fig. 9, which is less than the correlation length of water molecules σ_{OO} (3.17 Å), it is obvious that there is not enough room to accommodate the water molecules in the central minima region. As a result, a tubelike structure of water molecules is formed in the mouth region of the SWCNT and this type of structure is maintained also within the SWCNT, as

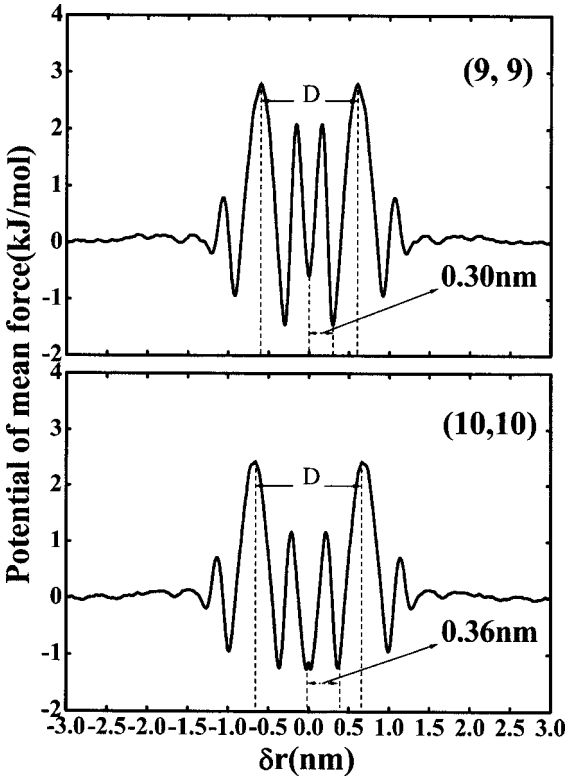

FIG. 9. The PMF of water along the radial direction for SWCNTs of (9, 9) and (10, 10). The *D* is the distance between the two outer maxima, which should equal to the diameter of SWCNT in an ideal situation.

shown in Fig. 7. Therefore, it is more favorable for the water molecules to form the solidlike phase within the pore region when the diameter of SWCNT is smaller than that of the (9, 9) SWCNT because of the spatial constraint. As the diameter of SWCNT increases, the minima distance of the PMF also increases, for example, the minima distance is around 0.36 nm for the (10, 10) SWCNT as shown in Fig. 9, as compared to 0.3 nm for the (9, 9) SWCNT, this distance is larger than the correlation length of water molecules, thus the water molecules can easily diffuse into the interior of the tubelike structure formed by water molecules, finally, these configurations will gradually approach the liquidlike phase. The behavior of water molecules in the extending region near the ends of SWCNT can give some hints to those dynamic and structural properties of water confined within the SWCNT.

IV. CONCLUSION

In our simulations, we did not try to avoid the stage in which the water is filling into the SWCNTs even though the structures in the interior are far away from their stable points. On the contrary, the structural properties of water near the end of SWCNT in this stage have been studied. The angle between dipole moment of water and the axle of SWCNT can be considered as a quantitative description for structural rearrangement of water molecules in the region where the water molecules are preparing to enter into the pore region of SWCNT since the symmetry is broken along the axle of SWCNT.

In the growth stage, we found that the region near the lower end of SWCNT with small diameters is a transitional zone which facilitates the water molecules to enter into the pore region of SWCNT from the bulk. In this region, the water molecule needs to rearrange its orientation to further adapt to the constraint environment. As the diameter of SWCNT increases, owing to the gradual weakening of size constraint, the orientation constraint of the water molecules in the transitional region also gradually weakens. When the extending distance is larger than 3.3 Å, the distribution and orientation properties of water molecules are similar to those near the graphite-water interface or in radial direction,[29] and the size constraint effect will be drastically reduced.

The water molecules will relax and rearrange to their stable configurations as the filling stage ends. These steady states are similar to those reported previously. The structural properties of water molecules in the vestibules at the openings of the SWCNTs with various diameters have also been studied by using the PMF analysis. We have demonstrated that these ambient structural properties can indirectly reflect their properties inside the nanotube, and the properties at nanometer scale are closely related to the size-constraint effect. Simulation results showed that there exists a close correlation between the PMF analysis and our results of MD simulations.

ACKNOWLEDGMENTS

The authors are grateful to Professor Lei Jiang for many stimulating discussions. This work was supported by NSFC (Grant Nos. 10425420 and 20773145), the Ministry of Science and Technology of China (Grant Nos. 2006CB806200 and 2006CB932100), as well as the Chinese Academy of Sciences including its CNIC supercomputer center.

[1] S. Iijima, Nature (London) **354**, 56 (1991).
[2] P. M. Ajayan and S. Iijina, Nature (London) **361**, 333 (1993).
[3] S. C. Tsang, Y. K. Chen, P. J. F. Harris, and M. L. H. Green, Nature (London) **372**, 159 (1994).
[4] C. Guerret-Plecourt, Y. L. Bouar, A. Loiseau, and H. Pascard, Nature (London) **372**, 761 (1994).
[5] C. H. Kiang, J. S. Choi, T. T. Tran, and A. D. Bacher, J. Phys. Chem. B **103**, 7449 (1999).
[6] G. Hummer, J. C. Rasaiah, and J. P. Noworyta, Nature (London) **414**, 188 (2001).
[7] A. Kalra, S. Garde, and G. Hummer, Proc. Natl. Acad. Sci. U.S.A. **100**, 10175 (2003).
[8] C. Dellago, M. M. Naor, and G. Hummer, Phys. Rev. Lett. **90**, 105902 (2003).
[9] G. M. Preston, T. P. Carroll, W. B. Guggino, and P. Agre, Science **256**, 385 (1992).
[10] Y. Gogotsi, J. A. Libera, A. Guvenc-Yazicioglu, and C. M. Megaridis, Appl. Phys. Lett. **79**, 1021 (2001).
[11] K. Koga, G. T. Gao, H. Tanaka, and X. C. Zeng, Nature (London) **412**, 802 (2001).
[12] M. C. Gordillo and J. Marti, Chem. Phys. Lett. **329**, 341 (2000).
[13] O. Beckstein, P. C. Biggin, and M. S. P. Sansom, J. Phys. Chem. B **105**, 12902 (2001).
[14] R. Allen, S. Melchionna, and J.-P. Hansen, Phys. Rev. Lett. **89**, 175502 (2002).
[15] A. Berezhkovskii and G. Hummer, Phys. Rev. Lett. **89**, 064503 (2002).
[16] Y. Liu and Q. Wang, Phys. Rev. B **72**, 085420 (2005).
[17] S. Sriraman, I. G. Kevrekidis, and G. Hummer, Phys. Rev. Lett. **95**, 130603 (2005).
[18] F. Zhu and K. Schulten, Biophys. J. **85**, 236 (2003).
[19] B. Huanga, Y. Xia, M. Zhao, F. Li, X. Liu, Y. Ji, and C. Song, J. Chem. Phys. **122**, 084708 (2005).
[20] U. Zimmerli, P. G. Gonnet, J. H. Walther, and P. Koumoutsakos, Nano Lett. **5**, 1017 (2005).
[21] K. Koga, H. Tanaka, and X. C. Zeng, Nature (London) **408**, 564 (2000).
[22] A. Striolo, A. A. Chialvo, K. E. Gubbins, and P. T. Cummings, J. Chem. Phys. **122**, 234712 (2005).
[23] W. H. Noon, K. D. Ausman, R. E. Smalley, and J. Ma, Chem. Phys. Lett. **355**, 445 (2002).
[24] R. J. Mashl, S. Joseph, N. R. Aluru, and E. Jakobsson, Nano Lett. **3**, 589 (2003).
[25] L. Feng, Z. Zhang, Z. Mai, Y. Ma, B. Liu, L. Jiang, and D. Zhu, Angew. Chem., Int. Ed. **43**, 2012 (2004).
[26] X. Feng, J. Zhai, and L. Jiang, Angew. Chem., Int. Ed. **44**, 5115 (2005).
[27] L. Jiang, Y. Zhao, and J. Zhai, Angew. Chem., Int. Ed. **43**, 4338 (2004).
[28] S. Wang, X. Feng, J. Yao, and L. Jiang, Angew. Chem., Int. Ed. **45**, 1264 (2006).
[29] J. H. Walther, R. Jaffe, T. Halicioglu, and P. Koumoutsakos, J. Phys. Chem. B **105**, 9980 (2001).
[30] T. Werder, J. H. Walther, R. L. Jaffe, T. Halicioglu, F. Noca, and P. Koumoutsakos, Nano Lett. **1**, 697 (2001).
[31] S. Vaitheeswaran, H. Yin, J. C. Rasaiah, and G. Hummer, Proc. Natl. Acad. Sci. U.S.A. **101**, 17002 (2004).
[32] A. Kutana and K. P. Giapis, Nano Lett. **6**, 656 (2006).
[33] I. Kosztin, B. Barz, and L. Janosi, J. Chem. Phys. **124**, 064106 (2006).
[34] A. R. Leach, *Molecular Modeling: Principles and Applications*, 2nd ed. (Prentice-Hall, Upper Saddle River, 2001).
[35] A. I. Kolesnikov, J.-M. Zanotti, C.-K. Loong, P. Thiyagarajan, A. P. Moravsky, R. O. Loutfy, and C. J. Burnham, Phys. Rev. Lett. **93**, 035503 (2004).
[36] A. V. Raghunathan and N. R. Aluru, Phys. Rev. Lett. **97**, 024501 (2006).
[37] C. Y. Won, S. Joseph, and N. R. Aluru, J. Chem. Phys. **125**, 114701 (2006).
[38] E. Lindahl, B. Hess, and D. van der Spoel, J. Mol. Model. **7**, 306 (2001).
[39] D. van der Spoel, E. Lindahl, B. Hess, A. R. van Buuren, E. Apol, P. J. Meulenhoff, D. P. Tieleman, A. L. T. M. Sijbers, K. A. Feenstra, R. van Drunen, and H. J. C. Berendsen, GROMACS User Manual, version 3.3 (2005).
[40] T. Darden, D. York, and L. Pedersen, J. Chem. Phys. **98**, 10089 (1993).
[41] U. Essmann, L. Perera, M. L. Berkowitz, T. Darden, H. Lee, and L. G. Pedersen, J. Chem. Phys. **103**, 8577 (1995).
[42] C. T. White, D. H. Robertson, and J. W. Mintmire, Phys. Rev. B **47**, 5485 (1993).
[43] C. Lobban, J. L. Finney, and W. F. Kuhs, J. Chem. Phys. **112**, 7169 (2000).
[44] C. G. Salzmann, P. G. Radaelli, A. Hallbrucker, E. Mayer, and J. L. Finney, Science **311**, 1758 (2006).
[45] I. Brovchenko, A. Geiger, and A. Oleinikova, J. Phys.: Condens. Matter **16**, S5345 (2004).
[46] P. Gallo, M. Rovere, and E. Spohr, J. Chem. Phys. **113**, 11324 (2000).
[47] M. C. Gordillo and J. Marti, Phys. Rev. B **75**, 085406 (2007).